

NASA/TM—2019-220209



# Vortex Radiometry: Enabling Frequency Agile Communications

*Peter J. Schemmel*  
*Glenn Research Center, Cleveland, Ohio*

## NASA STI Program . . . in Profile

Since its founding, NASA has been dedicated to the advancement of aeronautics and space science. The NASA Scientific and Technical Information (STI) Program plays a key part in helping NASA maintain this important role.

The NASA STI Program operates under the auspices of the Agency Chief Information Officer. It collects, organizes, provides for archiving, and disseminates NASA's STI. The NASA STI Program provides access to the NASA Technical Report Server—Registered (NTRS Reg) and NASA Technical Report Server—Public (NTRS) thus providing one of the largest collections of aeronautical and space science STI in the world. Results are published in both non-NASA channels and by NASA in the NASA STI Report Series, which includes the following report types:

- **TECHNICAL PUBLICATION.** Reports of completed research or a major significant phase of research that present the results of NASA programs and include extensive data or theoretical analysis. Includes compilations of significant scientific and technical data and information deemed to be of continuing reference value. NASA counter-part of peer-reviewed formal professional papers, but has less stringent limitations on manuscript length and extent of graphic presentations.
- **TECHNICAL MEMORANDUM.** Scientific and technical findings that are preliminary or of specialized interest, e.g., “quick-release” reports, working papers, and bibliographies that contain minimal annotation. Does not contain extensive analysis.
- **CONTRACTOR REPORT.** Scientific and technical findings by NASA-sponsored contractors and grantees.
- **CONFERENCE PUBLICATION.** Collected papers from scientific and technical conferences, symposia, seminars, or other meetings sponsored or co-sponsored by NASA.
- **SPECIAL PUBLICATION.** Scientific, technical, or historical information from NASA programs, projects, and missions, often concerned with subjects having substantial public interest.
- **TECHNICAL TRANSLATION.** English-language translations of foreign scientific and technical material pertinent to NASA's mission.

For more information about the NASA STI program, see the following:

- Access the NASA STI program home page at <http://www.sti.nasa.gov>
- E-mail your question to [help@sti.nasa.gov](mailto:help@sti.nasa.gov)
- Fax your question to the NASA STI Information Desk at 757-864-6500
- Telephone the NASA STI Information Desk at 757-864-9658
- Write to:  
NASA STI Program  
Mail Stop 148  
NASA Langley Research Center  
Hampton, VA 23681-2199

NASA/TM—2019-220209



# Vortex Radiometry: Enabling Frequency Agile Communications

*Peter J. Schemmel*  
*Glenn Research Center, Cleveland, Ohio*

National Aeronautics and  
Space Administration

Glenn Research Center  
Cleveland, Ohio 44135

---

May 2019

## Acknowledgments

This work is funded by the NASA Space Communication and Navigation Program, and is protected by a NASA New Technology Report and U.S. Provisional Patent.

Trade names and trademarks are used in this report for identification only. Their usage does not constitute an official endorsement, either expressed or implied, by the National Aeronautics and Space Administration.

*Level of Review:* This material has been technically reviewed by technical management.

Available from

NASA STI Program  
Mail Stop 148  
NASA Langley Research Center  
Hampton, VA 23681-2199

National Technical Information Service  
5285 Port Royal Road  
Springfield, VA 22161  
703-605-6000

This report is available in electronic form at <http://www.sti.nasa.gov/> and <http://ntrs.nasa.gov/>

# Vortex Radiometry: Enabling Frequency Agile Communications

Peter J. Schemmel  
National Aeronautics and Space Administration  
Glenn Research Center  
Cleveland, Ohio 44135

**Abstract:** Exponential proliferation of UAVs and CubeSats puts NASA's high priority communication systems at risk. UAVs and CubeSats are easy to acquire, modify and build, making it extremely likely that some will be used in unauthorized ways. While these systems provide several benefits to society, their increased use also increases the probability of unintentional signal interference, and even deliberate jamming of NASA's communication systems.

This paper presents an algorithm to determine 1) when an interference induced fade will occur, 2) how long the fade will persist for and 3) how intense the fade will be. The algorithm requires data collected from Vortex Radiometers (VRs), which probe the RF environment using annular antenna beam patterns. A set of numerical simulations show that a multi-beam VR system can instruct a cognitive antenna to switch between Ka- and X-Band communications, in order to avert interference from small diameter noise sources. Analysis of the simulation results indicate that practical VR systems will require several concentric annular beam patterns, in order to mitigate fades from noise sources of various sizes. The paper concludes by identifying technology challenges that need to be overcome to achieve these capabilities.

## 1. Introduction

The UAV and CubeSat marketplace is growing at a phenomenal rate, making it possible for small commercial entities, universities and even the public at large to become a part of the aerospace community [1–5]. These emerging markets have the potential to dramatically impact the world by providing new methods of disaster response, road traffic monitoring, farming, and even package delivery [6–11]. However, the growth in operational UAVs and CubeSats also creates challenges, especially for high priority communication systems.

Regulation of UAV and CubeSat communication systems is particularly challenging. These systems are easy to acquire, modify and build, and therefore their unauthorized use will undoubtedly occur. While countries around the world have agreed to international standards for the use of frequency spectrum, rogue UAV and CubeSats, can easily transmit on frequencies that are intended for other purposes. This could be accidental; a result of improper programming for example, or more nefarious.

The probability of a serious incident resulting from interference or jamming of a critical communication channel increases as proliferation of UAVs and CubeSats increases. For example, NASA's communication systems support space-vehicle launches, astronauts in orbit and critical science missions in deep space. Losing communication with any of these systems could result in loss of life, equipment and knowledge. NASA and other agencies must therefore develop robust countermeasures.

NASA is focused on developing cognitive antenna systems, in part to help tackle this problem. Simply put, a cognitive antenna can change its system parameters based on interactions with the environment in which it operates [12]. Some cognitive antennas are able to identify and mitigate interfering signals using adaptive filtering. Other cognitive systems aim to optimally allocate spectrum for multiple users.

While these systems are proving successful, many take the approach of analyzing real-time link statistics in order to predict future performance [13, 14]. Yet, fades on communication links due to adverse weather and signal interference are stochastic, which ultimately limits prediction

accuracy. Cognitive antenna capabilities will improve if interfering signals are identified and measured before they impact the communication link.

For example, interfering and jamming signals with large bandwidths and high power may not be mitigatable with adaptive filtering. In these situations, large scale changes in carrier frequency are required, such as transitioning from optical to RF, or from Ka- to X-Band. These types of frequency changes require time to bring the new systems online and coordinate between transmitter and receiver. Fortunately, Vortex Radiometers (VRs) are capable of providing advanced warning of impending fades. A new approach to analyzing VR data, in the limit of small diameter noise sources such as UAVs and CubeSats, is presented in this paper. This new approach estimates 1) when a fade will occur, 2) how long the fade will persist for and 3) how intense the fade will be. This information is then shared with cognitive antennas, which use it to determine when, and how to, carry out a frequency change.

## **2. Vortex Radiometry**

VRs create annular beam patterns by exploiting the orbital angular momentum (OAM) nature of electromagnetic fields [15, 16]. These annular beams measure radiometric data around a communication link, allowing VRs to detect noise sources before they interact with the link. Basic VR capability was demonstrated on a simulated 100 Mbps GEO-to-ground communication link, in a previous paper [17].

In those simulations, a noise source traversed across the communication beam, and without VR capabilities available, the link faded. However, when the VR was used, fade mitigation was successfully applied to maintain the link. The algorithm simply observed noise temperatures measured by the VR and communication link. If the noise temperature recorded by the VR was above some threshold temperature, fade mitigation was enabled. Mitigation was disabled when the VR noise temperature fell below the threshold AND the noise temperature measured by the communication link fell below the VR measured temperature. Previous VR simulations also showed that small noise sources, relative to the VR beam size, could slip past the detection algorithm. Reducing the azimuthal mode number of the VR beam, remedied the problem. However, this is a signal that multi-beam VRs should be considered.

UAVs and CubeSats fall into the small noise source category, and therefore mitigation of signal interference and jamming from these platforms requires multi-beam VR systems. While multi-beam VRs are more complex from a hardware perspective, they provide the ability to use more advanced fade detection algorithms. One example of an advanced algorithm is provided in the upcoming section. In it, noise sources are identified and their relative velocities are calculated. Analysis of the radiometric data then provides the ability to estimate 1) when the fade will occur, 2) how long the fade will persist for and 3) how intense the fade will be. Later on, this algorithm will be demonstrated on simulated Ka-Band communication link that switches to X-Band in order to avoid an interference induced fades.

## **3. Noise Source Parameter Estimation**

Changing frequency bands does not happen instantaneously. Efficient migration to a new band requires information about an impending noise source. Cognitive antennas need to know, for example, when to make the frequency change and how long to stay operating at the new frequency before it is safe to return. The intensity of the impending fade may also be a factor in determining the optimum fade mitigation strategy. The example algorithm provided here, is capable of providing this information to cognitive systems. For simplicity, a series of standard radiometers, producing Gaussian beam patterns (Fig. 1), are considered before introducing VRs. In either case, a minimum of two radiometer beams are required.

Identifying a noise source is the first step in the process, and is accomplished by monitoring sky brightness temperature with a radiometer. Under clear sky conditions, a radiometer will

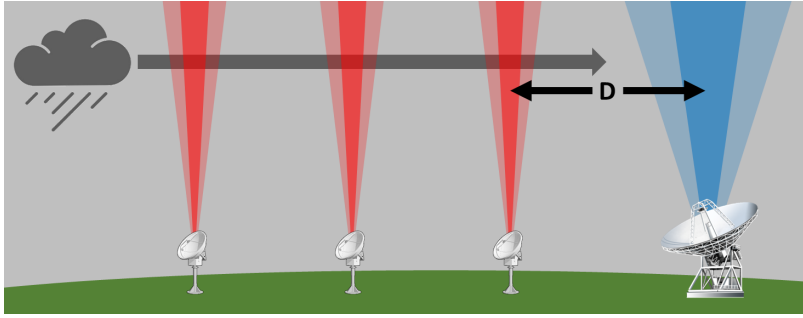


Fig. 1: Several cascaded radiometers determine noise source velocity and TOI from peaks in measured sky brightness temperature time series.

measure a constant brightness temperature, for fixed azimuth and elevation angles. However, measured brightness temperatures increase when rain, the Sun or an interfering signal passes through the antenna's beam pattern [18–21]. As the noise source vacates the beam, the brightness temperature returns to its clear sky value. The resulting temperature peak (Fig. 2), coupled with the known orientation of the radiometer determines the angular position of the noise source at a particular time. For simplicity, the remainder of this paper assumes that the altitude of the noise source is known. In practice this can be measured with a profiling radiometer, radar or a LIDAR system [22, 23]. The noise source has now been identified and located.

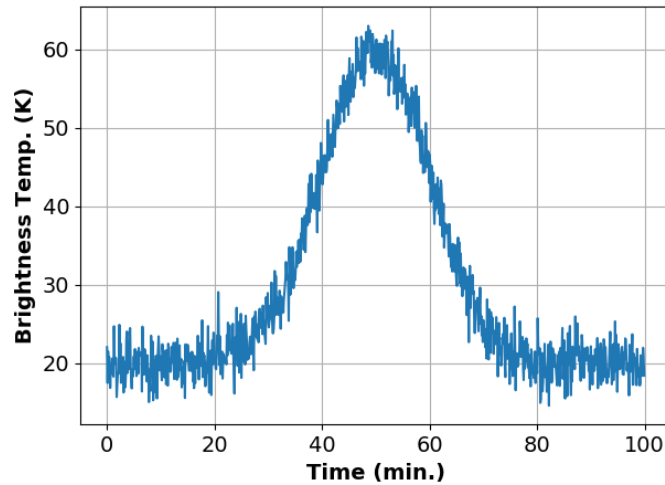


Fig. 2: Sky brightness temperature peak produced by a noise source traversing a radiometer's beam pattern.

Now that the noise source is identified, its velocity relative to the communication link must be measured. This is accomplished by identifying the source with a second radiometer using the same pointing angle as the first, but displaced by a known linear distance (Fig. 1). The relative velocity of the noise source is then,

$$V_{est} = \frac{D_{n+1} - D_n}{t_{n+1} - t_n}. \quad (1)$$

Again, for the purposes of this paper, it is assumed that the altitude of the noise source is known. In that case,  $D_n$  is the distance between the points of maximum gain of the  $n^{th}$  and  $n^{th} + 1$  radiometer, at the altitude of interest, and  $t_n$  is the time at which the noise source was identified. Adding additional radiometers along the path provides for several measurements to be averaged, resulting in a statistical distribution of possible velocities. When the relative velocity and distance from the noise source to the communication link ( $D_A$ ) are known, it is possible to calculate the time-of-impact (TOI).

$$TOI = \frac{D_A - D_n}{V_{est}} + t_n \quad (2)$$

TOI indicates when the maximum noise temperature will be recorded by the communication link. However, TOI on its own does not indicate when the fade will start or end. This requires an estimate of the fade persistence, or how long it will remain over the communication link.

Estimating fade persistence requires knowledge of 1) the minimum sky brightness temperature that will cause the communication link to fade, 2) how that temperature relates to the temperature recorded by the radiometers and finally 3) how long did the radiometers record noise temperatures above that threshold. The noise temperature limit that will cause the communication link to fade is,

$$T_{Lim} = \frac{P_{RF} \cdot G_R}{k_b \cdot R_{sRF} \cdot EsNO_{Req}}, \quad (3)$$

where  $P_{RF}$  is the RF signal power at the receiver,  $G_R$  is the receiver gain,  $k_B$  is Boltzmann's constant,  $R_{sRF}$  is the symbol rate (sym/sec) and  $EsNO_{Req}$  is the EsNO required to close the link.

If the radiometer and communication antenna patterns are the same,  $T_{Lim}$  is the same for both systems. However, if the beam patterns differ, the temperatures measured by the radiometer will not necessarily be equal to the temperatures seen by the communication link. A good estimator relating the  $T_{Lim}$  to the measured radiometer temperatures was found to be,

$$T_{VR_{Lim}} = \frac{I_{VR}}{I_{Comm}} \cdot (T_{Lim} - T_{sky}) + T_{sky}. \quad (4)$$

Here  $T_{Sky}$  is the clear sky brightness temperature, while  $I_{VR}$  and  $I_{Comm}$  are the peak gains of the radiometer and communication beam patterns, respectively. The time over which the VR measures an identified noise source temperature above  $T_{VR_{Lim}}$  is denoted  $\Delta t$ , and is the first parameter required to determine fade persistence (Fig. 3).

The final parameter required in order to estimate fade persistence is the relative width of the radiometer to communication antenna beams. This is calculable from knowledge of the antenna far-field beam patterns. This ratio  $R_w$  is found by first determining the antenna pattern with the lowest peak gain  $G_{Min}$ . The gain threshold is then taken to be half of the peak gain.

$$G_{Thres} = 0.5 \cdot G_{Min}. \quad (5)$$

The beam diameter  $\Theta$ , is then calculated for each antenna at  $G_{Thres}$ . This results in a width ratio of,

$$R_w = \frac{\Theta_{VR}}{\Theta_{Comm}}. \quad (6)$$

Finally, the fade persistence is estimated with,

$$t_{persist} = \frac{\Delta t}{R_w}. \quad (7)$$

Impact initiation time (IIT) or the time at which the communication link begins to fade is then,



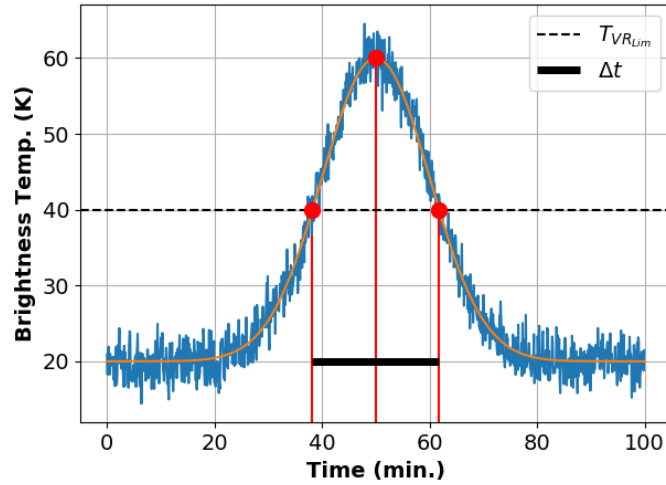


Fig. 3: Sky brightness temperature peak produced by a noise source traversing a radiometer's beam pattern.

$$IIT = TOI - 0.5 \cdot t_{persist}. \quad (8)$$

And the impact release time (IRT), or the time at which the communication link will no longer be in a fade, is simply,

$$IRT = TOI + 0.5 \cdot t_{persist}. \quad (9)$$

When the fade will occur and how long the fade will persist for, are now known. The final parameter estimation required is the fade intensity. The first step is to estimate the anticipated noise temperature that will be seen by the communication link by re-writing Eq. (4).

$$T_{est} = \frac{I_{comm}}{I_{VR}} \cdot (T_{VR} - T_{sky}) + T_{sky} \quad (10)$$

Readings from several radiometers can be averaged to produce a statistical probability distribution of  $T_{est}$ , resulting in a better estimate. The impact of the anticipated temperature increase, on the communication link's power margin is determined by recalculating the receiver carrier to noise ratio.

$$RCoNO' = \frac{P_{RF}}{T_{est} + k_b} \quad (11)$$

The reduced EsNO becomes,

$$EsNO' = \frac{RCoNO'}{R_{sRF}} \quad (12)$$

Which makes the anticipated link margin,

$$\Delta' = 10 \log_{10} \left( \frac{EsNO'}{EsNO_{Req}} \right) \quad (13)$$

The communication link will be under a fade if the reduced link margin  $\Delta'$  is negative.

While this set of equations was developed by envisioning a set of standard radiometers, with Gaussian antenna patterns displaced linearly from a communication link, they are also applicable to VRs (Fig. 4). However, the annual beam structure associated with VRs creates some additional effects that should be considered.

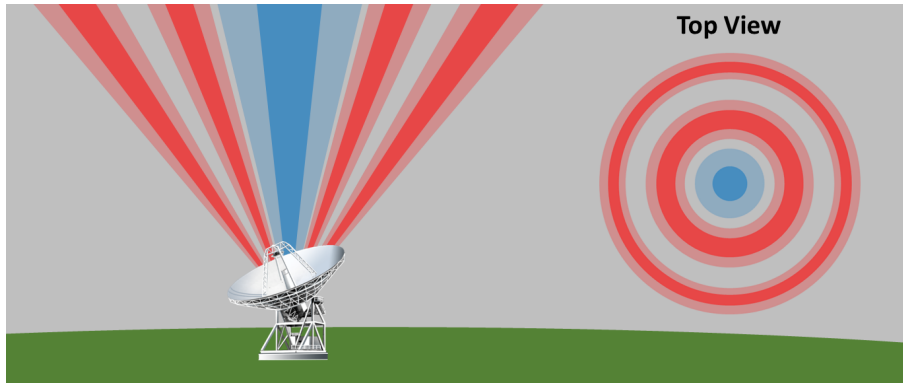


Fig. 4: Concentric annular radiometric beam patterns are used to determine fade characteristics prior to a noise source impinging upon the communication link. These parameters are then used to employ an optimal fade mitigation technique.

The primary issue in regards to using annular VR beams is that noise sources with relatively large diameters will skew the measured noise temperature time series. This is a fundamental result of overlapping an annulus with a circle. A circle of small diameter intersecting a larger annular beam is similar to using a standard Gaussian beam pattern, and produces symmetric peaks. However, as the circle's diameter increases, the peak temperature shifts towards the center of the annulus. This effect is demonstrated in Fig. 5.

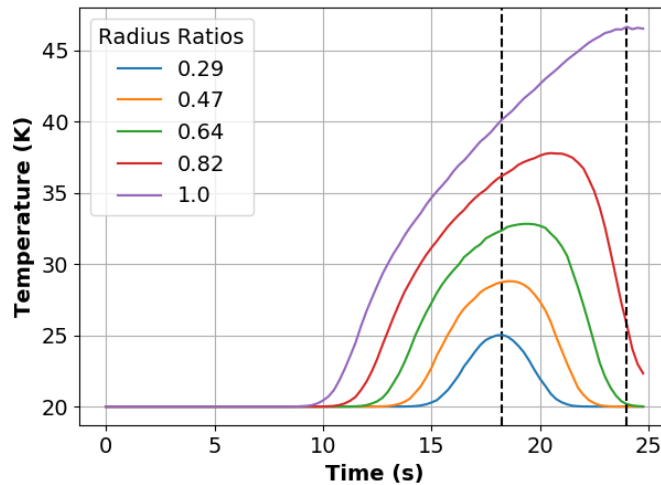


Fig. 5: Several noise temperature time series are shown for different ratios of noise source radius to annular beam radius. It is clear that the time series skews inward as the ratio is increased.

Increased skewness in the measured noise temperature time series results in improper determination of the time at which the noise source is over points of maximum antenna gain.

This adversely impacts the relative velocity (Eq. 1) and TOI (Eq. 2) estimates. Figure 5 shows that skewness increases as the ratio of noise source radius to maximum intensity radius, of the OAM beam, increases. The radius of maximum intensity of an OAM beam is [24],

$$r_{max} = \omega \sqrt{\frac{|l|}{2}}. \quad (14)$$

Here  $\omega$  is the beam radius [25]. Therefore, the impact of skewness can be reduced by increasing the azimuthal mode number associated with the VR antenna pattern. It is clear from this result, that multi-beam VR systems are required to detect noise sources of various sizes.

The set of equations within this section provide a means to estimate 1) when a fade will occur, 2) how long with will persist for and 3) how intense the fade will be. These estimations are valid for noise sources with effective radii that are less than the maximum intensity radius of the OAM mode used in the VR. Therefore, the parameter estimation is well suited to detecting small noise sources such as UAVs and CubeSats, which pose a particularly difficult challenge to high priority communication systems. The following section will demonstrate the effectiveness of this estimation routine by simulating a 100 Mbps, Ka-Band, GEO-to-ground communication link. A multi-beam VR will track a small noise source, detect the impending fade and instruct the Ka-Band link to change frequency band, in order to maintain the link.

#### 4. Simulation

The proliferation of UAVs and CubeSats poses an interference risk to high priority communication systems. Fortunately, data gathered by VRs can be used to estimate noise source characteristics and supply relevant parameters to a cognitive antenna, which will apply appropriate fade mitigation. This section demonstrates how VRs help cognitive antennas change frequency bands to advert fade events.

**Simulated Communication Link Parameters**

Parameter	Ka-Band		X-Band	
	Value	Units	Value	Units
Frequency	26	GHz	10	GHz
Transmitter Power	0.75	W	0.75	W
Transmitter Aperture Diameter	0.55	m	0.55	m
Modulation	BPSK	-	BPSK	-
Coding Scheme	Uncoded	-	Uncoded	-
Data Rate	100	Mbps	100	Mbps
BER	1E-6	-	1E-6	-
Range	35786	km	35786	km
Receiver Aperture Diameter	1.2	m	4	m
Sky Brightness Temperature	40	K	40	K
Sky Brightness Temperature Standard Deviation	0.25	K	0.25	K

Table 1

In this simulation, a primary 100 Mbps, Ka-Band, GEO-to-ground link is used in conjunction with a dual beam VR. A secondary, co-located, X-Band system is available to take over communications in case the Ka-Band link fails. Table 1 details the parameters of both links.

**Noise Source Parameters**

Parameter	Value	Units
Equivalent Brightness Temperature	800	K
Radius	15, 30 , 50	m
Velocity	100	m/s

Table 2

A noise source, with parameters outlined in Table 2, traverses across the Ka-Band link. Without VR capabilities enabled, the Ka-Band link undergoes a fade and data transmission is disabled. However, when VR capabilities are utilized, the noise source parameters are estimated using the equations given above. Doing so alerts the cognitive antenna controlling communications to the impending fade. At the appropriate time, the cognitive antenna changes operations to the X-Band system, maintaining data throughput while the noise source is obscuring the Ka-Band link.

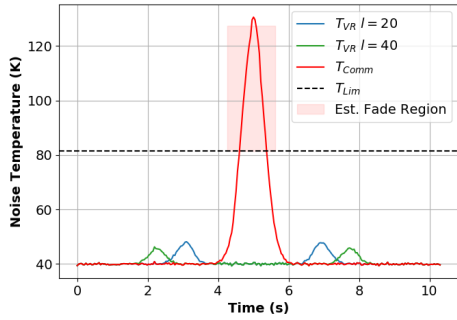
Simulation results are shown in Fig. 6, while parameter estimations are compared to actual values in Table 3. Take, for example, Fig. 6a. Here, measured noise temperature data is shown as a function of time. Twin noise temperature peaks are visible in both VR channels, a result of the annular beam pattern. The central peak,  $T_{Comm}$  is the noise temperature present on the communication link, and  $T_{Lim}$  (Eq. 3) is the noise temperature above which the Ka-Band link will fade. The shaded red region denotes the region in time that the VR system estimates a fade will occur. The top of the shaded region shows the anticipated noise temperature associated with the fade. Figure 6b displays link power margins for the Ka-Band system (red dashed line) and the Ka-/X-Band system (black line). It is clear from the figure that without the cognitive antenna orchestrating a frequency change, the Ka-Band link experiences a fade. Conversely, the Ka-/X-Band link, when instructed by the VR system, is able to avert the noise source induced fade.

Figure 6f shows that the VR estimated fade region becomes asymmetrical about the peak  $T_{Comm}$  noise temperature. This is not due to the parameter estimate degrading, as is evident by Table 3. Instead it is a result of the decreasing effective distance between the VR and communication link noise temperature peaks. As this effective distance decreases, a result of the noise source radius increasing, the parameter estimate is completed a later time. This is due to the need for the VR noise temperature to fall below  $T_{VRLim}$ , such that a  $\Delta t$  value (Eq. 7) may be calculated. In the case of Fig. 6e, fade mitigation is applied immediately after the parameter estimation is completed.

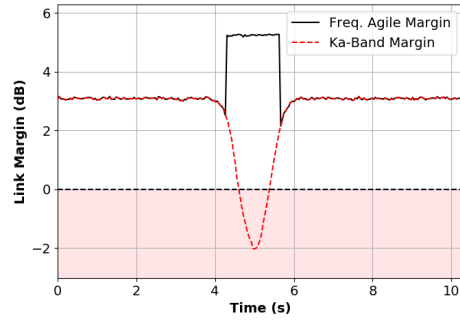
The asymmetry is reduced by increasing the azimuthal mode number of the VR system. This is demonstrated in Fig. 7, where the azimuthal mode number for both VR beams was increased from 20 and 40, to 40 and 60. It is clear from Fig. 7a that the noise temperature peaks are detected earlier, which allows the parameter estimation routine to complete at an earlier time. This produces a more symmetrical link power margin during the frequency switch to X-Band (Fig. 7b).

## 5. Conclusion

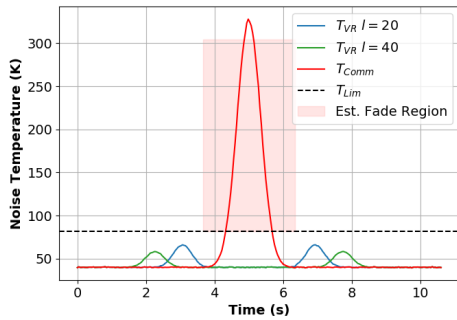
This paper shows that noise source parameters can be extracted from noise temperature time series data measured with VR systems. Cognitive antennas can take advantage of these parameters to



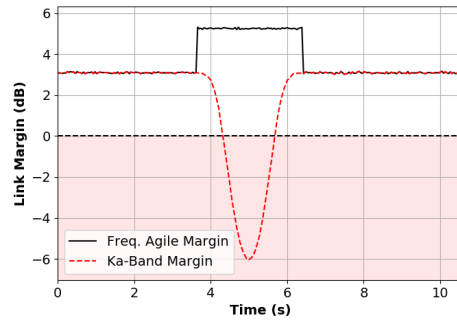
(a) Time series noise temperature data for a noises source with a 15m radius.



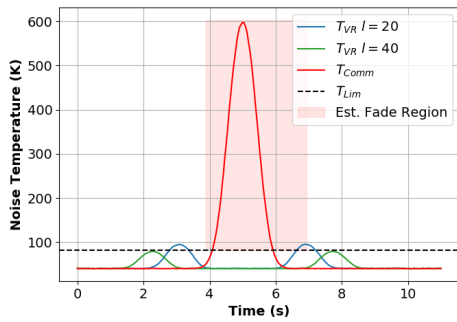
(b) Link power margins with and without fade mitigation enabled, in the presence of a 15m radius noise source.



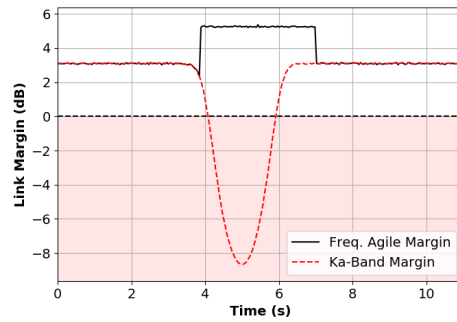
(c) Time series noise temperature data for a noises source with a 30m radius.



(d) Link power margins with and without fade mitigation enabled, in the presence of a 30m radius noise source.

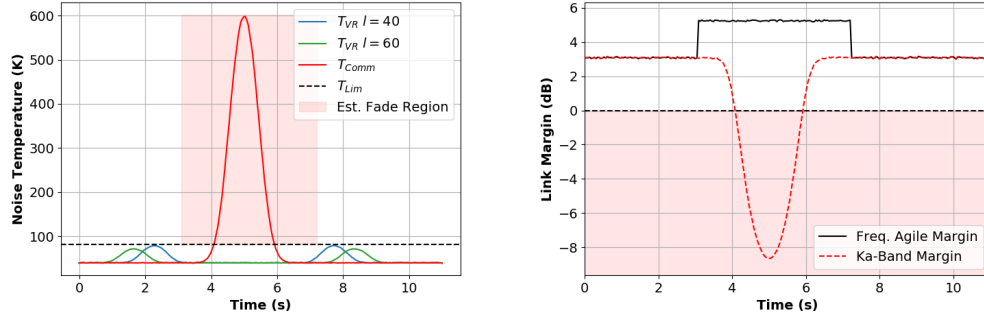


(e) Time series noise temperature data for a noises source with a 50m radius.



(f) Link power margins with and without fade mitigation enabled, in the presence of a 50m radius noise source.

Fig. 6: VRs utilize time series noise temperature data to estimate 1) when a fade will occur, 2) how long the fade will persist for and 3) how intense the fade will be. This data is then used to enable a frequency change, from Ka- to X-Band, in order to mitigate the fade.



(a) Time series noise temperature data for a noise source with a 50m radius and increased VR beam diameters. (b) Link power margins with and without fade mitigation enabled, in the presence of a 50m radius noise source radius and increased VR beam diameters.

Fig. 7: Identifying large diameter noise sources requires large diameter VR beams, in order to maintain a symmetrical link margin about the fade center.

**Noise Source Estimated Parameters**

Noise Source Radius		15m		30m	
Parameter	Units	Estimation	Actual	Estimation	Actual
Velocity	m/s	101.79	100	98.91	100
Brightness Temperature	K	127.34	130.47	303.78	328.05
TOI	s	4.96	5.01	5.02	4.98
Persistence	s	1.37	0.77	2.74	1.36
Noise Source Radius		50m		50m Revised	
Parameter	Units	Estimation	Actual	Estimation	Actual
Velocity	m/s	100.61	100	100.25	100
Brightness Temperature	K	602.67	597.64	600.77	597.67
TOI	s	5.01	5.04	5.02	5.04
Persistence	s	3.96	1.84	4.47	1.84

Table 3

efficiently employ fade mitigation. This is especially useful in the case of small noise sources such as UAVs and CubeSats, which pose particular interference challenges to high priority communication systems.

In both this paper, and “Vortex Radiometry: Fundamental Concepts,” the importance of multi-beam VR systems was noted. It is now apparent that any future implementation of VR systems must have multi-beam capabilities. A new technology development effort should be initiated in order to achieve practical multi-beam VRs. This effort must develop phase modulating devices (such as SPPs) that are capable of producing aberration free annular beam patterns. This will require the development of high precision modulators that reduce dispersion of the

OAM mode spectrum. Research should also be focused on increasing the sensitivity of VRs by developing high gain radiometers with large bandwidths. This is especially important for VRs producing large annular beam patterns, because their gain sensitivity is spread over a large area, thereby reducing their sensitivity to small noise sources.

Achieving these research objectives will enable next generation communication systems to base their fade mitigation strategies on measured environmental data. Proliferation of UAVs and CubeSats will make assuring link availabilities over 99% a challenge. Furthermore, designing communication link margins based on statistical climate data is going to become less reliable as global climate patterns shift. VRs will provide cognitive antennas with measured data, to keep high priority communication links available whenever needed.

## References

1. K. Herrick, "Development of the unmanned aerial vehicle market: forecasts and trends," *Air & Space Eur.* **2**, 25 – 27 (2000).
2. C. A. Wargo, G. C. Church, J. Glaneueski, and M. Strout, "Unmanned Aircraft Systems (UAS) research and future analysis," in *2014 IEEE Aerospace Conference*, (2014), pp. 1–16.
3. K. Woellert, P. Ehrenfreund, A. J. Ricco, and H. Hertzfeld, "Cubesats: Cost-effective science and technology platforms for emerging and developing nations," *Adv. Space Res.* **47**, 663 – 684 (2011).
4. J. Bouwmeester and J. Guo, "Survey of worldwide pico- and nanosatellite missions, distributions and subsystem technology," *Acta Astronaut.* **67**, 854 – 862 (2010).
5. R. Sandau, "Status and trends of small satellite missions for earth observation," *Acta Astronaut.* **66**, 1 – 12 (2010).
6. I. Colomina and P. Molina, "Unmanned aerial systems for photogrammetry and remote sensing: A review," *ISPRS J. Photogramm. Remote. Sens.* **92**, 79 – 97 (2014).
7. C. A. Rokhmana, "The potential of UAV-based remote sensing for supporting precision agriculture in indonesia," (2015), pp. 245 – 253. The 1st International Symposium on LAPAN-IPB Satellite (LISAT) for Food Security and Environmental Monitoring.
8. J. P. Dash, M. S. Watt, G. D. Pearse, M. Heaphy, and H. S. Dungey, "Assessing very high resolution UAV imagery for monitoring forest health during a simulated disease outbreak," *ISPRS J. Photogramm. Remote. Sens.* **131**, 1 – 14 (2017).
9. T. Ishida, J. Kurihara, F. A. Viray, S. B. Namuco, E. C. Paringit, G. J. Perez, Y. Takahashi, and J. J. Marciano, "A novel approach for vegetation classification using UAV-based hyperspectral imaging," *Comput. Electron. Agric.* **144**, 80 – 85 (2018).
10. S. R. Tsitas and J. Kingston, "6U CubeSat commercial applications," *The Aeronaut. J.* **116**, 189–198 (2012).
11. J. Dickinson, C. DeForest, and T. Howard, "The CubeSat Heliospheric Imaging Experiment (CHIME)," in *2011 Aerospace Conference*, (2011), pp. 1–12.
12. FCC Spectrum Policy Task Force, "Report of the spectrum efficiency working group," *Tech. Rep.* (2002).
13. M. M. J. L. van de Kamp, "Short-term prediction of rain attenuation using two samples," *Electron. Lett.* **38**, 1476–1477 (2002).
14. B. Gremont, M. Filip, P. Gallois, and S. Bate, "Comparative analysis and performance of two predictive fade detection schemes for Ka-band fade countermeasures," *IEEE J. on Sel. Areas Commun.* **17**, 180–192 (1999).
15. P. Schemmel, G. Pisano, and B. Maffei, "Modular spiral phase plate design for orbital angular momentum generation at millimetre wavelengths," *Opt. Express* **22**, 14712–14726 (2014).
16. P. Schemmel, S. Maccalli, G. Pisano, B. Maffei, and M. W. R. Ng, "Three-dimensional measurements of a millimeter wave orbital angular momentum vortex," *Opt. Lett.* **39**, 626–629 (2014).
17. P. Schemmel, "Vortex Radiometry: Fundamental Concepts," NASA Tech. Memo. 2019-xxxxxx (2019).
18. J. Nessel, M. Zemba, and J. Morse, "Results from three years of Ka-band propagation characterization at Svalbard, Norway," in *2015 9th European Conference on Antennas and Propagation (EuCAP)*, (2015), pp. 1–5.
19. M. Zemba, J. Nessel, J. Houts, N. Tarasenko, S. Lane, and D. Murrell, "Preliminary results from the AFRL-NASA W/V-band terrestrial link experiment in Albuquerque, NM," in *2016 IEEE International Symposium on Antennas and Propagation (APSURSI)*, (2016), pp. 1249–1250.
20. M. A. Janssen, *Atmospheric Remote Sensing By Microwave Radiometry* (New York: John Wiley, 1993).
21. T. Y. Otoshi, *Noise Temperature Theory and Applications for Deep Space Communication Antenna Systems* (Boston, Massachusetts: Artech House, 2008).
22. Z. Wang, X. Cao, L. Zhang, J. Notholt, B. Zhou, R. Liu, and B. Zhang, "Lidar measurement of planetary boundary layer height and comparison with microwave profiling radiometer observation," *Atmospheric Meas. Tech.* **5**, 1965–1972 (2012).
23. J. H. Churnside, T. A. Stermitz, and J. A. Schroeder, "Temperature profiling with neural network inversion of microwave radiometer data," *J. Atmospheric Ocean. Technol.* **11**, 105–109 (1994).
24. M. J. Padgett, F. M. Miatto, M. P. J. Lavery, A. Zeilinger, and R. W. Boyd, "Divergence of an orbital-angular-momentum-carrying beam upon propagation," *New J. Phys.* **17**, 023011 (2015).
25. P. F. Goldsmith, *Quasioptical Systems : Gaussian Beam Quasioptical Propagation and Applications* (New Jersey : IEEE Press, 1998).







